



ELSEVIER

Available online at www.sciencedirect.com

SCIENCE @ DIRECT®

Surface Science 521 (2002) 77–83



www.elsevier.com/locate/susc

Growth, electronic properties and thermal stability of the Fe/Al₂O₃ interface

A. Arranz^{a,b}, V. Pérez-Dieste^b, C. Palacio^{a,*}

^a *Departamento de Física Aplicada, Facultad de Ciencias, C-XII, Universidad Autónoma de Madrid, Cantoblanco, 28049 Madrid, Spain*

^b *LURE, Centre Universitaire Paris-Sud, Bât. 209 D, B.P. 34, 91898 Orsay Cedex, France*

Received 9 July 2002; accepted for publication 15 September 2002

Abstract

Soft X-ray photoelectron spectroscopy and resonant photoemission have been used to study the growth and electronic properties of Fe ultrathin films deposited on Al₂O₃ substrates. A simultaneous multilayer growth mode has been found for Fe growth at room temperature. For iron coverages below 1 ML, Fe²⁺ species are formed at the Fe/Al₂O₃ interface, followed by the formation of a metallic iron overlayer. The bonding of Fe at very low coverages occurs by charge transfer from Fe to surface oxygen atoms, and neither hybridisation of Fe and Al states nor reduction of the Al₂O₃ substrate are observed. The thermal stability of the interface has been also studied in the range 673–873 K. Annealing produces Fe agglomeration in such a way that some areas of the Al₂O₃ substrate become fully Fe-depleted. In these Fe-depleted areas, Fe²⁺ completely disappears and Al⁰ reduced species are formed. This behaviour would explain the decrease in the magnetoresistance performance of magnetic tunnel junctions after annealing above 573 K.

© 2002 Elsevier Science B.V. All rights reserved.

Keywords: Growth; X-ray photoelectron spectroscopy; Photoemission (total yield); Metallic films; Magnetic films; Iron; Aluminum oxide

1. Introduction

During the last years there has been an increasing interest in the study of metal–ceramic systems as a consequence of their use in a variety of technologies requiring specific electronic, optical, magnetic, mechanical or catalytic properties [1–13]. The above-mentioned properties of metal–ceramic components are in general strongly affected by the

interfacial microstructure and chemical composition at the interface.

In order to understand bonding and adhesion mechanisms and other phenomena that are specific of the metal–ceramic interfaces, several fundamental studies have been carried out recently on interfaces formed by growing ultrathin metallic layers of different metals on oxide substrates [1]. In particular, ultrathin iron films grown on Al₂O₃ surfaces have a great potential in the field of nanoscale magnetism, where the Fe/Al₂O₃/Fe system is used as a magnetic tunnel junction (MTJ). The magnetoresistance of such MTJ's depends critically on the spin polarisation at the interfaces between the magnetic film and the insulator layer,

* Corresponding author. Tel.: +34-91-3975266; fax: +34-91-3974949.

E-mail address: carlos.palacio@uam.es (C. Palacio).

and therefore on the composition and sharpness of the interface [14–16]. In spite of its promising interest not only in magnetic but also in catalytic applications, only few studies on the formation of the Fe/Al₂O₃ interface are available [17,18].

In this work we present a study of the growth and electronic properties of Fe ultrathin films deposited on Al₂O₃ substrates at room temperature (RT), by means of soft X-ray photoelectron spectroscopy (SXPS) and resonant photoemission (RPE). We also analyse the thermal stability of the interface up to 873 K.

2. Experimental

The experiments were performed at LURE (Orsay, France) using the PES2 experimental station connected to the SU8 undulator beamline of the Super-Aco storage ring. The measurements were carried out in a purpose-built ultrahigh vacuum system, with a base pressure better than 1×10^{-10} Torr, equipped with an angle resolving 50 mm hemispherical VSW analyser coupled on a goniometer inside the chamber. For a photon energy ($h\nu$) of 150 eV, the overall energy resolution, including the analyser, was estimated to be better than 100 meV. Photoemission spectra have been normalised to the incident current measured in a gold grid located at the entrance of the chamber.

The Al₂O₃ substrate was made by annealing (~ 723 K) an aluminium-foil substrate of 99.994% purity in 5N oxygen at a partial pressure of 1×10^{-5} Torr for about 30 min. Complete oxidation was assured by the absence of a metallic component in the Al2p band. Iron was evaporated by electron bombardment of a high purity Fe-wire target at constant heating power, in such a way that the thickness of the Fe layer is controlled by the deposition time. During Fe evaporation the residual pressure was always kept below 1×10^{-9} Torr.

3. Results and discussion

3.1. Deposition at room temperature

Fig. 1 shows (a) the Al2p, (b) Fe 3p and (c) valence band (VB) spectra measured with $h\nu =$

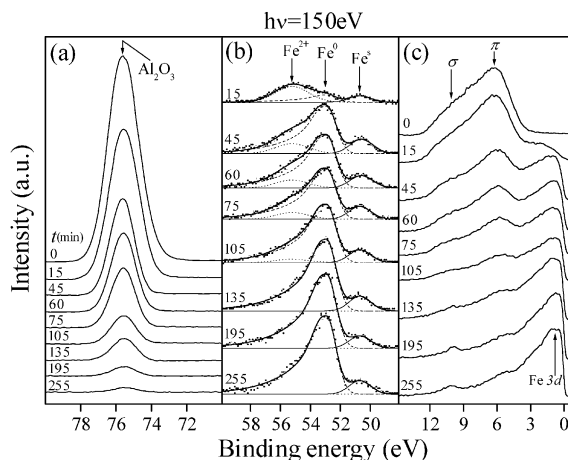


Fig. 1. Photoemission spectra measured with $h\nu = 150$ eV of (a) Al2p band, (b) Fe 3p band, and (c) VB, respectively, for different iron deposition times. The deconvolution of Fe 3p spectra carried out as explained in the text is also shown.

150 eV for different iron deposition times, after background subtraction based on a modified Shirley method [19]. The spectra labelled $t = 0$ min are representative of the Al₂O₃ substrate. The Al2p is characterised by a single symmetric band, and no reduced Al species are observed in the low binding energy side upon iron deposition. The Al2p spectra have been aligned at 75.6 eV, as observed in Fig. 1(a), using the applied energy shift to correct surface charging effects in the Fe 3p and VB spectra. The full width at half-maximum of the Al2p band at 0 min is 2 eV, decreasing to 1.6 eV at 45 min. This decrease is a consequence of the formation of an iron-conducting layer on the surface which leads to a more homogeneous surface potential [20]. With increasing iron deposition time, the Al2p strongly attenuates and practically disappears for higher deposition times.

For small deposition times, the Fe 3p band shows a complex shape. In particular, for $t = 15$ min, the main peak of the Fe 3p band is observed at ~ 55.2 eV, being attributed to the formation of Fe²⁺ species during the very first stages of the Fe/Al₂O₃ interface formation [13]. With increasing Fe deposition time, the Fe²⁺ peak strongly attenuates and an asymmetric peak at 53 eV, that can be attributed to the formation of metallic iron, Fe⁰, emerges. In addition to that, another peak, Fe^δ,

can be observed at 50.7 eV for all deposition times. The separation between the Fe^s and Fe^0 peaks is independent of the photon energy, therefore indicating that the Fe^s peak should be associated to a photoemission peak rather than to an Auger transition. The intensity of Fe^s peak remains nearly constant for $t \geq 45$ min. This behaviour suggests that Fe^s species are located at the surface, and probably correspond to Fe atoms with a lower atomic coordination, that is to surface atoms in the outer atomic layer. The deconvolution of the Fe 3p spectra in terms of Fe^0 , Fe^{2+} and Fe^s components is illustrated in Fig. 1(b).

The VB spectra of the Al_2O_3 substrate is characterised by two broad peaks at ~ 6.2 and 10 eV, that are attributed to π and σ molecular orbitals, respectively, formed by hybridisation of Al 3sp and O 2p atomic orbitals [21]. It should be pointed out that the Al_2O_3 VB of the thermal film presents a bandgap greater than 3 eV with no electronic states. Since oxygen vacancies are characterised by the formation of occupied states between 2–3 eV [9,22], this should indicate the formation of a highly stoichiometric oxide film. During iron deposition, a strong attenuation of the π and σ peaks as well as the growth of the metallic Fe 3d band at ~ 0.8 eV below the Fermi level, E_F , are observed.

Fig. 2 shows the normalised Al 2p (■) and total Fe 3p (●) signal intensities as a function of iron deposition time. In addition, the Fe^0 , Fe^{2+} and Fe^s signal intensities obtained from the deconvolution of spectra in Fig. 1(b) are also shown. With increasing iron deposition time, the Al 2p band strongly attenuates and nearly disappears for higher deposition times, therefore suggesting that the Al_2O_3 surface is completely covered with iron. This behaviour rules out either Volmer Weber (VW) or Stranski-Krastanov (SK) growth modes [11,23]. On the other hand, the continuous variation of the Al 2p and Fe 3p signals to reach saturation suggests a simultaneous multilayer (SM) growth mode, rather than pure layer-by-layer. In this model iron condensates in layers in such a way that at a layer starts to grow before the preceding layer is completed. Therefore, the surface consists on a series of terraces at different atomic levels [24]. According to the SM growth mode, the Al

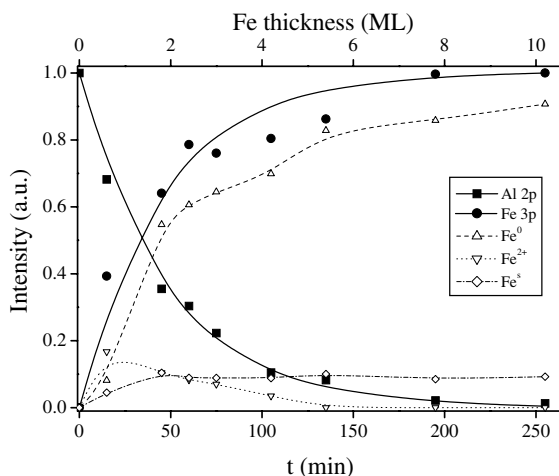


Fig. 2. Normalised Al 2p (■) and total Fe 3p (●) signal intensities as a function of iron deposition time. The evolution of the Fe^0 , Fe^{2+} and Fe^s signal intensities obtained from the deconvolution of spectra in Fig. 1(b) are also shown.

and total Fe normalised intensities can be described by Eqs. (1) and (2), respectively [23]

$$I_{\text{Al}} = \exp\left(\frac{-a_{\text{Fe}}Rt}{\lambda_{\text{Al}}^{\text{Fe}} \cos \varphi}\right) \quad (1)$$

$$I_{\text{Fe}} = 1 - \exp\left(\frac{-a_{\text{Fe}}Rt}{\lambda_{\text{Fe}}^{\text{Fe}} \cos \varphi}\right) \quad (2)$$

where $\lambda_{\text{Fe}}^{\text{Fe}}$ and $\lambda_{\text{Al}}^{\text{Fe}}$ are the attenuation lengths of Fe 3p and Al 2p photoelectrons in Fe, respectively, R is the evaporation rate in ML/min, φ is the take-off angle, and $a_{\text{Fe}} \approx 2.3 \text{ \AA}$ is the iron monolayer thickness. Eqs. (1) and (2) have been used to fit the data of Fig. 2, using R as the only adjustable parameter and assuming $\lambda_{\text{Fe}}^{\text{Fe}} = \lambda_{\text{Al}}^{\text{Fe}} = 4.4 \text{ \AA}$ [25]. Experimental measurements were carried out at normal emission, that is $\varphi = 0^\circ$. The best fit parameter is $R = 0.039 \text{ ML/min}$ for the Al 2p data and $R = 0.041 \text{ ML/min}$ for the Fe 3p data. Therefore, the evaporation rate, $R = 0.040 \pm 0.001 \text{ ML/min}$, was used to calibrate the top axis in Fig. 2.

VW-like growth mode has been reported for the growth of Ag, Pt, Pd, Rh, Co and Al on Al_2O_3 substrates [10], and its explanation was formulated in terms of surface free energy [1]. According to this criterion, a VW growth mode should be expected for the Fe/ Al_2O_3 system [1]. However, as

pointed out before, the Al and Fe signal evolutions of Fig. 2 allow to rule out such a growth mode. The SM growth mode has been also observed during the growth of vanadium oxide on Al_2O_3 [20]. Such a type of growth mode is indicative of very low or negligible lateral mobility of the atoms impinging on the surface. To our knowledge, this is the first time that the growth mode of Fe deposited on Al_2O_3 substrates at RT has been determined.

It is well established that the affinity of the deposited metal to oxygen is a crucial factor determining the interaction strength at the metal/oxide interface, the wetting characteristics of the deposited metal, and the mechanical properties of the interface [3,10]. A strong interaction between Fe, at low fractional monolayer coverages, and TiO_2 and MnO substrates has been observed in the literature [12,13]. In particular, Diebold et al. [13] have observed the formation of an oxidized-Fe-reduced- TiO_2 interface followed by the formation of a metallic Fe overlayer during the growth of Fe on $\text{TiO}_2(110)$ substrates at RT. The oxidation of several metals (Ti, Nb, V, Cr, Ni, Cu) supported on alumina substrates has been also observed [5,6,8–10]. Ealet and Gillet [9] have found that metals with low electronegativity like Cr or Ni promote the formation of an oxide phase at the interface, whereas atoms with a higher electronegativity (close to oxygen) induce an electronic transfer from the oxide substrate to the metal deposit. Varma et al. [6] have found that Cu donates charge to surface oxygen with the formation of Cu–O bonds at the Cu/ Al_2O_3 interface, being the reaction layer limited to one atomic layer. In contrast with TiO_2 , Al_2O_3 cannot be easily reduced. However, Al reduced species have been observed during Ti and Nb deposition on Al_2O_3 substrates at RT [5]. For iron (see Fig. 1(b)), the formation of Fe^{2+} species takes place during the first deposited Fe ML, as expected from the high chemical reactivity of iron to oxygen, but no Al reduction can be observed in Fig. 1(a), in good agreement with the Auger electron spectroscopy (AES) results of Colaianni et al. [17]. A theoretical study of Johnson and Pepper [2] on the interfaces between alumina and transition metals, using the molecular orbital approach, predicts that the d-

orbitals of the transition metals (Ag, Cu, Ni and Fe) may establish interactions with the p-orbitals of the O^{2-} anions of the Al_2O_3 surface, whereas interactions between the metal ions of the support and the deposited metal are not predicted. Therefore, as pointed out by Diebold et al. [13] for the Fe/ TiO_2 system, bonding of Fe at very low coverages should take place by charge transfer from Fe to surface oxygen atoms, whereas hybridisation of Fe and Al states should not take place. This is in agreement with results of Fig. 1, where Fe^{2+} species are formed for Fe coverages below 1 ML, but no reduction or formation of metallic Fe–Al species at lower binding energies can be observed.

3.2. Resonant photoemission

Further complementary information on the electronic structure of the deposited films can be obtained through RPE experiments. To carry out this task, VB spectra have been measured near the

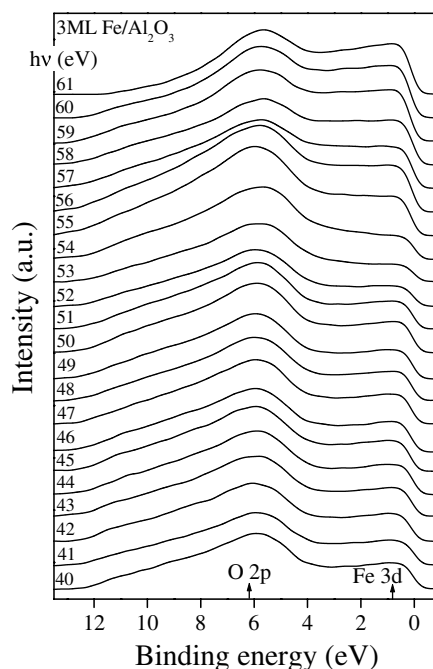


Fig. 3. VB spectra of a 3 ML Fe film deposited on stoichiometric Al_2O_3 as a function of the photon energy in the range $h\nu = 40\text{--}61$ eV.

Fe 3p \rightarrow 3d excitation threshold. Fig. 3 shows the VB spectra of an iron film 3 ML thick deposited on stoichiometric Al₂O₃ as a function of the binding energy, for different photon energies in the range $h\nu = 40\text{--}61$ eV. Spectra have been normalised to the incident photon flux. Similar series have been also measured for iron films of thickness 1.8 and 5.4 ML, respectively. RPE is usually interpreted as due to the interference between the direct photoemission process from the Fe 3d levels, $3p^63d^n + h\nu \rightarrow 3d^{n-1} + e^-$, and the autoionization emission of a highly localised excited state created by photoabsorption, $3p^63d^n + h\nu \rightarrow [3p^53d^{n+1}]^* \rightarrow 3p^63d^{n-1} + e^-$ [26]. In iron oxides, RPE is explained as due to the hybridisation between the O 2p and Fe 3d orbitals and therefore RPE can be used to isolate the Fe 3d-derived states contribution to the VB [27].

Constant-initial-state (CIS) curves of (a) Fe 3d states at ~ 0.8 eV, and (b) O 2p derived states at ~ 6.2 eV below E_F for the 1.8, 3 and 5.4 ML Fe films deposited on Al₂O₃ at RT are shown in Fig. 4. The shape of the CIS curves for the Fe 3d states is similar to that observed by Kaurila et al. [28] on bulk iron and iron thin films deposited on Cu substrates, in good agreement with the mainly metallic behaviour observed in the Fe 3p spectra of the Fe films thicker than 1 ML. A careful analysis of the position of the destructive minimum before

the enhancing resonance carried out fitting the data of Fig. 4(a), in the range $h\nu = 51\text{--}55$ eV, to a parabola shows that the minimum is at 53.5 eV for the film 1.8 ML thick and at 52.7 eV for the films 3 and 4.5 ML thick. Since FeO_x single crystals have Fe 3d-derived states at ~ 1.2 eV below E_F that show resonance profiles characterised by a minimum at $h\nu = 54$ eV [27], the above-mentioned difference should be attributed to the initial formation of Fe²⁺ species for low iron coverages. With increasing the film thickness, the influence of Fe²⁺ species in the resonance profile decreases in such a way that the minimum of the CIS curve shifts to lower energies to reach the expected value for metallic iron [27,28].

As shown in Fig. 4(b), a resonance is observed at $h\nu = 55$ eV for the O 2p VB derived states for the different Fe films. According to previous published results [29], the metallic Fe MVV Auger transition overlaps with the O 2p derived states at $h\nu \sim 55\text{--}56$ eV, and therefore the observed resonance in Fig. 4(b) should be attributed to the Fe MVV Auger transition, especially for higher Fe thicknesses when the contribution of metallic iron becomes dominant. However, the intensity of the resonance is practically independent on the Fe thickness. This fact suggests that for low Fe coverages (1.8 ML), the resonance should be also related to the Fe²⁺ species, since the FeO_x VB has Fe 3d-derived states at ~ 6.9 eV that present a maximum in their resonance profile at $h\nu = 57$ eV [27].

3.3. Thermal annealing

It has been reported that annealing MTJ's up to ~ 503 K strongly increases the magnetoresistance performance of the device, being the Al₂O₃ barrier height and effective thickness also modified [30,31]. The origin of the annealing enhancing effect is related to the modification of the interface between the ferromagnetic electrode and the insulating barrier layer [31]. However, for annealing temperatures above 573 K, the magnetoresistance performance is degraded. According to Keavney et al. [31], this behaviour suggests that some disorder created during deposition is annealed out, up to a certain optimal temperature, at which point

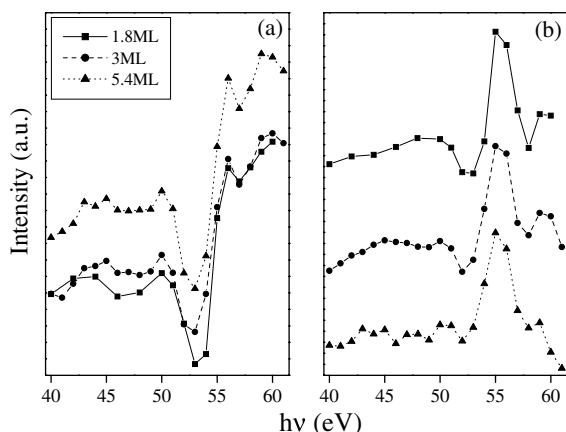


Fig. 4. CIS curves of (a) Fe 3d states at ~ 0.8 eV, and (b) O 2p derived states at ~ 6.2 eV below E_F for the Fe films 1.8, 3 and 5.4 ML thick deposited on Al₂O₃ at RT.

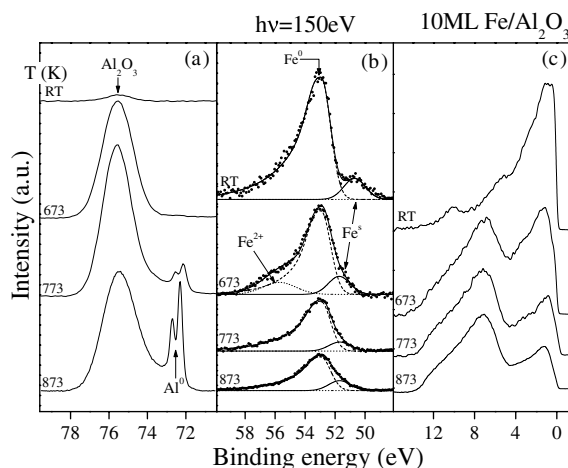


Fig. 5. Photoemission spectra measured with $h\nu = 150$ eV of (a) Al 2p band, (b) Fe 3p band, and (c) VB, respectively, of a 10 ML Fe film on Al_2O_3 measured after annealing during 15 min at 673, 773 and 873 K. Spectra measured after deposition at RT are also given for comparison.

other processes begin to reduce the spin-polarised current.

In order to get more insight into the processes taking place at the interface during annealing above the optimal temperature (~ 503 K), we have studied the thermal stability of the Fe/ Al_2O_3 interface in the temperature range of 673–873 K. Fig. 5 shows (a) the Al 2p, (b) the Fe 3p and (c) the VB spectra measured with $h\nu = 150$ eV of an iron film 10 ML thick deposited on Al_2O_3 . Measurements were carried out after annealing during 15 min at 673, 773 and 873 K. Spectra measured at RT are also given for comparison. The deconvolution of the Fe 3p spectra is illustrated in Fig. 5(b). With increasing temperature, the Al 2p and O 2p VB states related to the Al_2O_3 substrate increase considerably. Also a decrease of the Fe 3p and Fe 3d VB intensities is observed. It is important to note that Fe^{2+} species appears with annealing at 673 K. Above this temperature, Fe^{2+} species disappear, along with the formation of Al^0 reduced species in the low binding energy side of the Al 2p band. The annealing also produces a shift of ~ -1 eV of the Fe^s peak, therefore suggesting an increase of the atomic coordination of the outer Fe surface atoms probably due to the agglomeration of Fe.

Colaianni et al. [17] have studied, using AES and high resolution electron energy loss spectroscopy, the thermal modification of the Fe(3.2 Å)/ Al_2O_3 (18.5 Å) interface deposited on a Mo(110) substrate in the temperature range 90–1200 K. According to these authors, annealing up to 900 K causes agglomeration of Fe leading to large clusters, in such a way that the Al_2O_3 substrate is reexposed in some areas after annealing. Such process (Ostwald ripening) has been also observed during annealing of Cu films deposited on TiO_2 [32]. Since the diffusion coefficient of Fe on Al_2O_3 , $D \sim 10^{-20}$ $\text{cm}^2 \text{s}^{-1}$ at ~ 873 K [33], is too small to explain the decrease of iron species and the increase of the aluminium oxide species, respectively, the above-mentioned agglomeration should be responsible for the evolution of the Al 2p, Fe 3p and VB spectra in Fig. 5. At ~ 673 K, Fe begins to agglomerate into larger clusters, being the Al_2O_3 substrate and the Fe^{2+} species formed during the first stages of Fe deposition reexposed in some areas. Above this temperature, annealing causes further agglomeration of iron in such a way that the Fe^{2+} species are destroyed and Al^0 reduced species are formed in Fe-depleted areas. It should be pointed out that the AES results of Colaianni et al. [17] do not show the reduction of the Al_2O_3 oxide in their Fe/ Al_2O_3 interface. However, in our case it exists a straightforward connection between the elimination of Fe^{2+} species and the reduction of the Al_2O_3 substrate in the Fe-depleted areas. A rough estimation of the Al_2O_3 substrate reexposed area calculated from the Al 2p signal intensity gives $\sim 50\%$ at 873 K. The above-mentioned modification of the Fe/ Al_2O_3 interface could explain the reduction in the magnetoresistance performance of MTJ devices with annealing above the optimal temperature.

4. Conclusions

SXPS and RPE have been used to study the growth and electronic properties of Fe ultrathin films deposited on Al_2O_3 substrates at RT. A SM growth mode has been found for Fe growth. For iron coverages below 1 ML, Fe^{2+} species are formed at the Fe/ Al_2O_3 interface, followed by the

formation of a metallic iron overlayer. Bonding of Fe at very low coverages occurs by charge transfer from Fe to surface oxygen atoms, whereas hybridisation of Fe and Al states does not take place. No reduction of the Al₂O₃ substrate upon iron deposition at RT is observed.

The thermal stability of the interface has been examined above the optimal annealing temperature reported in the literature for MTJ devices. Results are consistent with the Fe agglomeration to form large clusters. As a consequence of Fe agglomeration, some areas become fully Fe-depleted, in such a way that Fe²⁺ species are eliminated and Al⁰ reduced species are formed in these areas. This annealing behaviour of the Fe/Al₂O₃ interface could explain the decrease in the magnetoresistance performance of MTJ devices when annealed above their optimal temperature.

Acknowledgements

A part of this work has been financially supported by the Large Scale Facilities of the European Community to LURE, project no. ES814-01. One of us (A. Arranz) acknowledges financial support from the Spanish Ministerio de Educación y Cultura.

References

- [1] C.T. Campbell, Surf. Sci. Rep. 27 (1997) 1, and references therein.
- [2] K.H. Johnson, S.V. Pepper, J. Appl. Phys. 53 (1982) 634.
- [3] M.W. Finnis, J. Phys. Condens. Matter 8 (1996) 5811.
- [4] C. Verdozzi, D.R. Jennison, P.A. Schultz, M.P. Sears, Phys. Rev. Lett. 82 (1999) 799.
- [5] F.S. Ohuchi, M. Kohyama, J. Am. Ceram. Soc. 74 (1991) 1163.
- [6] S. Varma, G.S. Chottiner, M. Arbab, J. Vac. Sci. Technol. A 10 (1992) 2857.
- [7] S.M. Mukhopadhyay, C.S. Chen, J. Vac. Sci. Technol. A 10 (1992) 3545.
- [8] B. Ealet, E. Gillet, V. Nehasil, P.J. Møller, Surf. Sci. 318 (1994) 151.
- [9] B. Ealet, E. Gillet, Surf. Sci. 367 (1996) 221.
- [10] M. Bäumer, J. Biener, R.J. Madix, Surf. Sci. 432 (1999) 189, and references therein.
- [11] S. Andersson, P.A. Brühwiler, A. Sandell, M. Frank, J. Libuda, A. Giertz, B. Brena, A.J. Maxwell, M. Bäumer, H.J. Freund, N. Märtensson, Surf. Sci. 442 (1999) L964.
- [12] V. Di Castro, G. Polzonetti, S. Ciampi, G. Contini, O. Sahko, Surf. Sci. 293 (1993) 41.
- [13] U. Diebold, H. Tao, N.D. Shinn, T.E. Madey, Phys. Rev. B 50 (1994) 14474.
- [14] H. Chen, Q.Y. Xu, G. Ni, J. Lu, H. Sang, S.Y. Zhang, Y.W. Du, J. Appl. Phys. 85 (1999) 5798.
- [15] R. Schad, K. Mayen, J. McCord, D. Allen, D. Yang, M. Tondra, D. Wang, J. Appl. Phys. 89 (2001) 6659.
- [16] S.R. Teixeira, M.A.S. Boff, W.H. Flores, J.E. Schmidt, M.C.M. Alves, H.C.N. Tolentino, J. Magn. Magn. Mater. 233 (2001) 96.
- [17] M.L. Colaianni, P.J. Chen, J.T. Yates, Surf. Sci. 238 (1990) 13.
- [18] H. Poppa, C.A. Papageorgopoulos, F. Marks, E. Bauer, Z. Phys. D 3 (1986) 279.
- [19] A. Proctor, M.P.A. Sherwood, Anal. Chem. 54 (1982) 13.
- [20] J. Biener, M. Bäumer, R.J. Madix, P. Liu, E.J. Nelson, T. Kendelewicz, G.E. Brown Jr., Surf. Sci. 441 (1999) 1.
- [21] S. Thomas, P.M.A. Sherwood, Anal. Chem. 64 (1992) 2488.
- [22] A. Arranz, V. Pérez-Dieste, C. Palacio, Phys. Rev. B 66 (2002) 075420.
- [23] C. Argile, G.E. Rhead, Surf. Sci. Rep. 10 (1989) 277.
- [24] M.G. Barthès, A. Rolland, Thin Solid Films 76 (1981) 45.
- [25] S. Tanuma, C.J. Powell, D.R. Penn, Surf. Interf. Anal. 17 (1991) 911.
- [26] L.C. Davis, J. Appl. Phys. 59 (1986) R25.
- [27] R.J. Lad, V.E. Henrich, Phys. Rev. B 39 (1989) 13478.
- [28] T. Kaurila, L. Säisä, J. Väyrynen, J. Phys. Condens. Matter 6 (1994) 5053.
- [29] H. Kato, T. Ishii, S. Masuda, Y. Harada, T. Miyano, T. Komeda, M. Onchi, Y. Sakisaka, Phys. Rev. B 32 (1985) 1992.
- [30] M. Sato, H. Kihuchi, K. Kobayashi, J. Appl. Phys. 83 (1998) 6691.
- [31] D.J. Keavney, S. Park, C.M. Falco, J.M. Slaughter, Appl. Phys. Lett. 78 (2001) 234, and references therein.
- [32] A.K. See, R.A. Bartynski, Phys. Rev. B 50 (1994) 12064.
- [33] O. Lenoble, J.F. Bobo, L. Hennet, H. Fischer, Ph. Bauer, M. Piecuch, Thin Solid Films 275 (1996) 64.